第 43 卷 第 12 期/2023 年 6 月/光学学报 研究论文

光学学报

海洋湍流下涡旋光束经粗糙面的回波特性

吴鹏飞[1*]，张咪[1]，王姣[2]，谭振坤[3]

[1]西安理工大学自动化与信息工程学院，陕西 西安 710048；

[2]陕西科技大学电子信息与人工智能学院，陕西 西安 710021；

[3]西安工业大学光电工程学院，陕西 西安 710021

摘要 光场回波散射特性是未来水下激光通信与探测一体化的关键技术之一，而具有螺旋波前结构的涡旋光束[如拉盖尔-高斯(LG)光束]更适合抑制海洋湍流的影响。利用广义Huygens-Fresnel原理，推导出弱海洋湍流中LG光束经高斯分布粗糙表面反射的回波散斑强度的解析表达式；数值分析了光源参数、海洋湍流以及粗糙目标表面参数对回波散斑场复相干度的影响。结果表明，复相干度随着LG光束拓扑荷数、束腰半径、波长的增大而减小，随着海洋湍流强度的增大而降低，随着粗糙面相干长度的增加而增大，并且当粗糙表面的相干长度大于球形波在海洋湍流中传播的相干长度时，复相干度变化不明显，表明此时粗糙表面对复相干度的影响远小于海洋湍流的影响。这一结论为海洋湍流条件下目标探测与识别提供了参考。

关键词 海洋光学；海洋湍流；拉盖尔-高斯光束；散斑；回波特性；复相干度

中图分类号 O436 **文献标志码** A **DOI**：10.3788/AOS222163

1 引 言

在海洋探测技术、水下散射技术和水下无线光通信技术中[1-2]，光束经海洋湍流的传输特性[3-6]以及湍流情况[7-8]下光束经粗糙面的回波特性发挥了重要作用。目前的水下探测技术主要以激光为主[9-11]，但激光在探测过程中的损耗严重，导致接收的散斑可以反映的粗糙目标信息有限。涡旋光束[12]具有空心光强分布、相位螺旋以及轨道角动量(OAM)正交等特点，相比高斯光束可以携带更多的信息。拉盖尔-高斯(LG)光束[13]是典型的涡旋光束，在光散射、目标识别等领域具有显著的优势[14]。

微观世界中大部分目标表面相对光波段来说是粗糙的且服从高斯分布[15]，光波照射粗糙面会产生随机反射，Goodman使用“随机行走”模型对光束的散斑现象进行详细解释[16]。根据波传播的随机散射理论[17]，涡旋光束经随机粗糙面散射，回波均产生散斑效应。目前对于光束经粗糙目标散射特性的研究主要集中在两个方面：第一，自由空间中光束经粗糙面的散斑特性。刘曼等[18-19]在自由空间中模拟了不同拓扑荷数的涡旋光束经随机粗糙表面散射后在衍射区形成的横向和纵向光强及相位分布。Holmes等[20]利用扩展的Huygens-Fresnel原理对湍流环境中传播的散斑强度的一阶和二阶统计量进行研究。Cui等[21]分析了涡旋光束被不同粗糙程度的表面散射产生的散斑模式，并与高斯光产生的散斑模式进行比较。第二，大气湍流中光束经粗糙面的散斑特性。Li等[22-24]基于Rytov近似，研究了大气湍流中LG光束被随机粗糙表面散射的回波特性。2022年，李艳玲等[25]对湍流大气中随机粗糙表面回波空间相干性进行仿真。目前涡旋光束经海洋湍流的传输理论[26-28]已经发展成熟，但对于海洋湍流中涡旋光束经高斯随机粗糙面的回波散射特性鲜有研究。

本文利用广义Huygens-Fresnel衍射原理，建立了海洋湍流中LG光束经高斯随机粗糙面的双程传输模型，推导了海洋湍流中LG光束经高斯随机粗糙面的回波光强以及回波光场复相干度，探究了光源参数、海洋湍流强度、粗糙面参数对复相干度的影响。

2 基本原理

2.1 LG光束的回波散射光强分布

建立海洋湍流下LG光束经粗糙面散射的双程传输模型，如图1所示，LG光束在海洋湍流中的传输路径分为从发射端到粗糙面的传输路径和从粗糙面到接

收稿日期：2022-12-21；**修回日期**：2023-01-12；**录用日期**：2023-03-12；**网络首发日期**：2023-03-25

基金项目：陕西省科技成果转移与推广计划项目(2020CGXNG-041)、陕西省教育厅服务地方专项计划项目(20JC027)、国家自然科学基金(62001363，62101313)、陕西省重点研发计划工业领域一般项目(2022GY-100)、陕西省科协青年人才支持项目(20220142)

通信作者：*wupengf@xaut.edu.cn

收端的回波路径，且都考虑海洋湍流对LG光束的相位扰动。LG光束从发射端A出发，通过海洋湍流到达距离为z处的粗糙面B，这个过程根据Rytov近似加载海洋湍流相位扰动，经粗糙面B反射，最后通过海洋湍流到达接收端C，此过程利用广义Huygens-Fresnel原理表示光束传输时受海洋湍流的相位扰动。

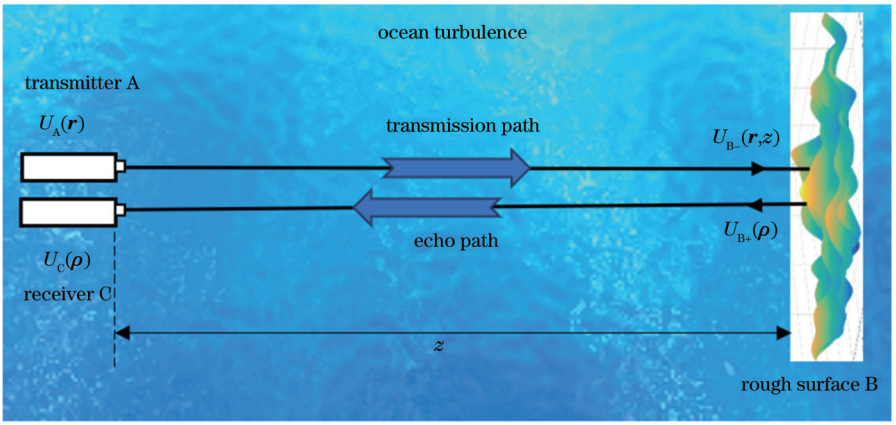

图1　海洋湍流中LG光束经粗糙面双程传输示意图

Fig. 1　Double-path propagation of LG beam through rough surface in ocean turbulence

在直角坐标系下，传输距离为z时LG光束的光场复振幅[29]为

$$U_A(\boldsymbol{r},z)=U_A(r,\theta,z)=\sqrt{\frac{2p!}{\pi(p+|l|)!}}\cdot\frac{1}{\omega(z)}\left[\frac{r\sqrt{2}}{\omega(z)}\right]^{|l|}L_p^{(l)}\left[\frac{2r^2}{\omega^2(z)}\right]\times\exp\left[\frac{-r^2}{\omega^2(z)}\right]\exp\left[\frac{-\mathrm{i}kr^2z}{2(z^2+z_R^2)}\right]\times\exp\left[\mathrm{i}(2p+|l|+1)\tan(z/z_R)\right]\exp(-\mathrm{i}l\theta),\quad(1)$$

式中：$\boldsymbol{r}=(r,\theta)$为二维矢量坐标；$\omega(z)=\omega_0[1+(z/z_R)^2]^{1/2}$为传输距离$z$处的光束半径，其中$\omega_0$为束腰半径；$k$为空间波束；i为虚数单位；$z_R=(\pi\omega_0^2)/\lambda$为瑞利距离，$\lambda$为波长；$L_p^{(l)}$为拉盖尔多项式，$l$和$p$分别为LG光束的拓扑荷数和径向指数。由于$p\neq0$时LG光束的光斑是径向多维的，在本文后续的研究中无法提供准确的闭合表达式，因此采用径向指数$p=0$的LG光束作为光源。图2为$l=2$的LG光束光强分布图。

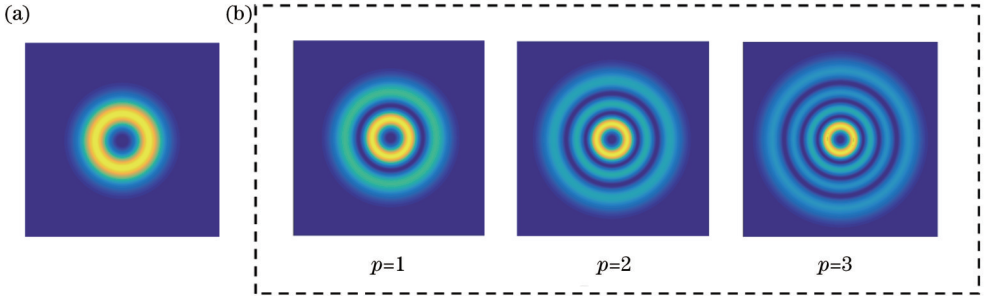

图2　拓扑荷数为2的LG光束光强分布图。(a) $p=0$；(b) $p\neq0$

Fig. 2　Intensity distribution of LG beam ($l=2$). (a) $p=0$; (b) $p\neq0$

根据Rytov近似[30]，LG光束通过海洋湍流后入射到粗糙面的光场为

$$U_{B-}(\boldsymbol{\rho},z)=U_A(\boldsymbol{r},0)\exp[\psi_1(\boldsymbol{\rho},\boldsymbol{r})],\quad(2)$$

式中：$\psi_1(\boldsymbol{\rho},\boldsymbol{r})$为发射端A到粗糙面B的海洋湍流复相位扰动；$\boldsymbol{\rho}$表示粗糙面B的二维坐标点；$\boldsymbol{r}$表示发射端A的二维坐标点。

高斯随机粗糙面的表面高度波动服从高斯分布。图3给出了由蒙特卡罗法生成的高斯随机粗糙面高度分布函数三维图，利用粗糙面的相干长度ρ_h控制粗糙面在横向的起伏量，并利用粗糙面的均方根粗糙度σ_h控制粗糙面的纵向起伏量。相干长度越小，或均方根

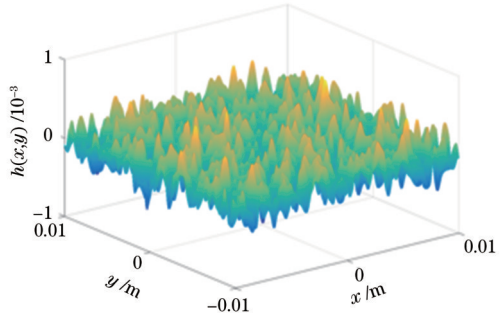

图3　高斯粗糙面的表面高度分布函数($\sigma_h=\lambda$，$\rho_h=20$ mm)

Fig. 3　Height distribution function of Gaussian rough surface ($\sigma_h=\lambda$, $\rho_h=20$ mm)

粗糙度越大，粗糙面的粗糙度越大[15]。

LG光束垂直入射到粗糙面B，粗糙面反射后的光场可以表示为

$$U_{B+}(\boldsymbol{\rho},z)=U_{B-}(\boldsymbol{\rho},z)\exp\left[\mathrm{i}\varphi(\boldsymbol{\rho})\right], \tag{3}$$

式中：$\varphi(\boldsymbol{\rho})=2kh(\boldsymbol{\rho})$为随机粗糙面引起的随机相位；$h(\boldsymbol{\rho})$为高斯粗糙面的表面高度分布函数。

LG光束经粗糙面散射的光场互相干函数[31]为

$$\left\langle U_{B+}(\boldsymbol{\rho}_1,z)U_{B+}^{*}(\boldsymbol{\rho}_2,z)\right\rangle=\left\langle U_{B-}(\boldsymbol{\rho}_1,z)\exp\left[\varphi(\boldsymbol{\rho}_1)\right]U_{B-}^{*}(\boldsymbol{\rho}_2,z)\exp\left[\varphi^{*}(\boldsymbol{\rho}_2)\right]\right\rangle=$$

$$\left\langle U_{B-}(\boldsymbol{\rho}_1,z)U_{B-}^{*}(\boldsymbol{\rho}_2,z)\right\rangle\times\left\langle\exp\left\{\mathrm{i}2k\left[h(\boldsymbol{\rho}_1)-h(\boldsymbol{\rho}_2)\right]\right\}\right\rangle=\left\langle U_{A}(\boldsymbol{r}_1,z)U_{A}^{*}(\boldsymbol{r}_2,z)\right\rangle\left\langle\exp\left[\psi_1(\boldsymbol{\rho}_1,\boldsymbol{r}_1)+\psi_1^{*}(\boldsymbol{\rho}_2,\boldsymbol{r}_2)\right]\right\rangle\times$$

$$\left\langle\exp\left\{\mathrm{i}2k\left[h(\boldsymbol{\rho}_1)-h(\boldsymbol{\rho}_2)\right]\right\}\right\rangle, \tag{4}$$

其中，粗糙面的相位扰动系综平均[24]为

$$\left\langle\exp\left\{\mathrm{i}2k\left[h(\boldsymbol{\rho}_1)-h(\boldsymbol{\rho}_2)\right]\right\}\right\rangle=2k\sigma_{h}\delta(\boldsymbol{\rho}_1-\boldsymbol{\rho}_2)\exp\left[(\boldsymbol{\rho}_1-\boldsymbol{\rho}_2)^{2}/\rho_{h}^{2}\right]。 \tag{5}$$

LG光束被随机粗糙面B反射后进入海洋湍流继续传播，最终到达接收端C。根据广义Huygens-Fresnel原理[32]，接收端的光场表达式为

$$U_{C}(\boldsymbol{p})=\frac{k\exp(\mathrm{i}kl)}{2\pi\mathrm{i}z}\int U_{B+}(\boldsymbol{\rho},z)\exp\left[\frac{\mathrm{i}k|\boldsymbol{p}-\boldsymbol{\rho}|^{2}}{2z}+\psi_2(\boldsymbol{p},\boldsymbol{\rho})\right]\mathrm{d}\boldsymbol{\rho}, \tag{6}$$

式中：$\psi_2(\boldsymbol{p},\boldsymbol{\rho})$为海洋湍流引起的相位扰动；$\boldsymbol{p}$为接收端的二维矢量坐标点。

回波光场的互相干函数[33]$\Gamma(\boldsymbol{p}_1,\boldsymbol{p}_2)$为

$$\Gamma(\boldsymbol{p}_1,\boldsymbol{p}_2)=\left\langle U_{C}(\boldsymbol{p}_1)U_{C}^{*}(\boldsymbol{p}_2)\right\rangle=\left(\frac{k}{2\pi z}\right)^{2}\iint\left\langle U_{B+}(\boldsymbol{\rho}_1)U_{B+}^{*}(\boldsymbol{\rho}_2)\right\rangle\times$$

$$\exp\left[-\frac{\mathrm{i}k\left(|\boldsymbol{p}_1-\boldsymbol{\rho}_1|^{2}-|\boldsymbol{p}_2-\boldsymbol{\rho}_2|^{2}\right)}{2z}\right]\left\langle\exp\left[\psi_2(\boldsymbol{p}_1,\boldsymbol{\rho}_1)+\psi_2^{*}(\boldsymbol{p}_2,\boldsymbol{\rho}_2)\right]\right\rangle\mathrm{d}\boldsymbol{\rho}_1\mathrm{d}\boldsymbol{\rho}_2。 \tag{7}$$

采用Rytov相位结构函数的二次近似，得到的海洋湍流系综平均[5]为

$$\left\langle\exp\left[\psi_1(\boldsymbol{\rho}_1,\boldsymbol{r}_1)+\psi_1^{*}(\boldsymbol{\rho}_2,\boldsymbol{r}_2)\right]\right\rangle=\exp\left[-0.5D_{\psi_1}(\boldsymbol{r}_1-\boldsymbol{r}_2)\right]\approx\exp\left[-\frac{(\boldsymbol{r}_1-\boldsymbol{r}_2)^{2}}{\rho_0^{2}}\right], \tag{8}$$

$$\left\langle\exp\left[\psi_2(\boldsymbol{p}_1,\boldsymbol{\rho}_1)+\psi_2^{*}(\boldsymbol{p}_2,\boldsymbol{\rho}_2)\right]\right\rangle\approx\exp\left[-\frac{(\boldsymbol{p}_1-\boldsymbol{p}_2)^{2}+(\boldsymbol{p}_1-\boldsymbol{p}_2)(\boldsymbol{\rho}_1-\boldsymbol{\rho}_2)+(\boldsymbol{\rho}_1-\boldsymbol{\rho}_2)^{2}}{\rho_0^{2}}\right], \tag{9}$$

式中：$D_{\psi 1}(\boldsymbol{r}_1-\boldsymbol{r}_2)$为海洋湍流中球面波的波结构常数；$\rho_0$为球面波在海洋湍流中传输的相干长度[34]。

$$\rho_0=\left[1.28k^{2}z\eta^{-1/3}C_n^{2}(6.78+47.57\omega^{-2}-17.67\omega^{-1})\right]^{-1/2}, \tag{10}$$

式中：$C_n^{2}=10^{-8}\chi_T\varepsilon^{-1/3}$为海洋湍流等效温度结构参数；$\chi_T$为温度方差耗散率，从海洋表面到深水层的取值为$10^{-10}\sim10^{-4}\ \mathrm{K^2/s}$；$\varepsilon$为湍流动能耗散率，取值范围为$10^{-10}\sim10^{-1}\ \mathrm{m^2/s^3}$；$\eta$为柯尔莫哥洛夫尺度，$\eta=10^{-3}$；$\omega$表征温度和盐度变化的相对强度，取值为$-5\sim0$。

将式(4)、(5)、(8)、(9)代入式(7)，得

$$\Gamma(\boldsymbol{p}_1,\boldsymbol{p}_2)=\left\langle U_{C}(\boldsymbol{p}_1)U_{C}^{*}(\boldsymbol{p}_2)\right\rangle=\left(\frac{k}{2\pi z}\right)^{2}\iint\left\langle U_{A}(\boldsymbol{r}_1,z)U_{A}^{*}(\boldsymbol{r}_2,z)\right\rangle\exp\left[-\frac{(\boldsymbol{r}_1-\boldsymbol{r}_2)^{2}}{\rho_0^{2}}\right]\times$$

$$2k\sigma_{h}\delta(\boldsymbol{\rho}_1-\boldsymbol{\rho}_2)\exp\left[\frac{(\boldsymbol{\rho}_1-\boldsymbol{\rho}_2)^{2}}{\rho_{h}^{2}}\right]\times\exp\left[-\frac{\mathrm{i}k\left(|\boldsymbol{p}_1-\boldsymbol{\rho}_1|^{2}-|\boldsymbol{p}_2-\boldsymbol{\rho}_2|^{2}\right)}{2z}\right]\times$$

$$\exp\left[-\frac{(\boldsymbol{p}_1-\boldsymbol{p}_2)^{2}+(\boldsymbol{p}_1-\boldsymbol{p}_2)(\boldsymbol{\rho}_1-\boldsymbol{\rho}_2)+(\boldsymbol{\rho}_1-\boldsymbol{\rho}_2)^{2}}{\rho_0^{2}}\right]\mathrm{d}\boldsymbol{\rho}_1\mathrm{d}\boldsymbol{\rho}_2。 \tag{11}$$

利用质心、差分坐标变换$2\boldsymbol{\rho}_c=\boldsymbol{\rho}_1+\boldsymbol{\rho}_2$、$\boldsymbol{\rho}_d=\boldsymbol{\rho}_1-\boldsymbol{\rho}_2$、$2\boldsymbol{p}_c=\boldsymbol{p}_1+\boldsymbol{p}_2$、$\boldsymbol{p}_d=\boldsymbol{p}_1-\boldsymbol{p}_2$对式(11)进行简化，得到

$$\Gamma(\boldsymbol{p}_1,\boldsymbol{p}_2)=\left(\frac{k}{2\pi z}\right)^2\frac{2}{\pi(|l|)!}\iint\frac{2^{|l|}}{\omega^{2|l|+2}(z)}\left(\boldsymbol{\rho}_{\mathrm{c}}+\frac{1}{2}\boldsymbol{\rho}_{\mathrm{d}}\right)^{|l|}\left(\boldsymbol{\rho}_{\mathrm{c}}-\frac{1}{2}\boldsymbol{\rho}_{\mathrm{d}}\right)^{|l|}\times$$
$$\exp\left[\frac{-\left(2\boldsymbol{\rho}_{\mathrm{c}}^2+\frac{1}{2}\boldsymbol{\rho}_{\mathrm{d}}^2\right)}{\omega^2(z)}\right]\exp\left(\frac{-\mathrm{i}k\boldsymbol{\rho}_{\mathrm{c}}\boldsymbol{\rho}_{\mathrm{d}}z}{z^2+z_{\mathrm{R}}^2}\right)\exp(-\mathrm{i}l\theta_{\mathrm{d}})\exp\left(-\frac{\boldsymbol{\rho}_{\mathrm{d}}^2}{\rho_0^2}\right)\times$$
$$2k\sigma_{\mathrm{h}}\exp\left(\frac{\boldsymbol{\rho}_{\mathrm{d}}^2}{\rho_{\mathrm{h}}^2}\right)\exp\left[-\frac{\mathrm{i}k}{z}(\boldsymbol{p}_{\mathrm{c}}\boldsymbol{p}_{\mathrm{d}}+\boldsymbol{\rho}_{\mathrm{c}}\boldsymbol{\rho}_{\mathrm{d}}-\boldsymbol{p}_{\mathrm{c}}\boldsymbol{\rho}_{\mathrm{d}}-\boldsymbol{p}_{\mathrm{d}}\boldsymbol{\rho}_{\mathrm{c}})\right]\times\exp\left(-\frac{\boldsymbol{p}_{\mathrm{d}}^2+\boldsymbol{p}_{\mathrm{d}}\boldsymbol{\rho}_{\mathrm{d}}+\boldsymbol{\rho}_{\mathrm{d}}^2}{\rho_0^2}\right)\mathrm{d}\boldsymbol{\rho}_{\mathrm{c}}\mathrm{d}\boldsymbol{\rho}_{\mathrm{d}},\tag{12}$$

式中：$\theta_{\mathrm{d}}=\theta_1-\theta_2$；$\exp(-\mathrm{i}l\theta_{\mathrm{d}})$为相位螺旋因子。

$$(x^2+y^2)^n=\sum_{m=0}^{n}\begin{bmatrix}n\\m\end{bmatrix}x^{2(n-m)}y^{2m},\tag{13}$$

$$\exp(-\mathrm{i}l\theta_{\mathrm{d}})=\begin{bmatrix}|l|\\s\end{bmatrix}\left[-\mathrm{isgn}(l)\right]^{(s)}\rho_{\mathrm{d}x}^{(|l|-s)}\rho_{\mathrm{d}y}^{(s)},\tag{14}$$

$$\int_{-\infty}^{\infty}x^n\exp(-ax^2+2bx)\mathrm{d}x=(2\mathrm{i})^{-n}\frac{\sqrt{\pi}}{\left(\sqrt{a}\right)^{n+1}}\exp\left(\frac{b^2}{a}\right)\mathrm{H}_n\left[\mathrm{i}\left(\frac{b}{\sqrt{a}}\right)\right],\ a>0,\tag{15}$$

$$\mathrm{H}_n(x_1)=\sum_{m=0}^{n/2}(-1)^m\frac{n!}{m!(n-2m)!}(2x_1)^{n-2m},\tag{16}$$

式中：m、s为大于等于0的整数；$\mathrm{sgn}(\cdot)$为符号函数；$\mathrm{H}_n(\cdot)$为n阶厄米特多项式；a和b表示任意参数。

利用式(13)～(16)的积分变换[35]对(12)式进行积分，得到

$$\Gamma(\boldsymbol{p}_1,\boldsymbol{p}_2,z)=\left\langle U_{\mathrm{C}}(\boldsymbol{p}_1)U_{\mathrm{C}}^{*}(\boldsymbol{p}_2)\right\rangle=\left(\frac{k^3\sigma_{\mathrm{h}}}{\pi\sqrt{\pi}\,z^2(|l|)!}\right)\frac{2^{-4|l|}}{\omega^{2|l|+2}(z)}\cdot\frac{\mathrm{i}^{-3|l|}}{\left(\sqrt{E}\right)^{|l|+2}}\exp\left\{-\frac{\mathrm{i}k}{z}\left[\frac{1}{2}(\boldsymbol{p}_1+\boldsymbol{p}_2)(\boldsymbol{p}_1-\boldsymbol{p}_2)\right]\right\}\times$$
$$\exp\left[-\frac{(\boldsymbol{p}_1-\boldsymbol{p}_2)^2}{\rho_0^2}\right]\sum_{m=0}^{|l|}\sum_{s=0}^{|l|}\sum_{k_1=0}^{2(|l|-m)}\sum_{e=0}^{2(|l|-m)}\begin{bmatrix}|l|\\m\end{bmatrix}\begin{bmatrix}|l|\\s\end{bmatrix}\begin{bmatrix}2(|l|-m)\\k_1\end{bmatrix}\begin{bmatrix}2(|l|-m)\\e\end{bmatrix}\times\frac{2^{-2m}}{\left(\sqrt{E}\right)^{4m}}\cdot\frac{\left[-\mathrm{isgn}(l)\right]^{(s)}}{\left[\sqrt{\frac{2}{\omega^2(z)}}\right]^{2(|l|-m)+1}}\times$$
$$\exp\left\{\frac{\left[B(\boldsymbol{p}_1-\boldsymbol{p}_2)\right]^2\omega^2(z)}{8}\right\}(2\mathrm{i})^{-k_1+2f-e+2g}\frac{1}{\left(\sqrt{E}\right)^{k_1-2f+e-2g}}\mathrm{H}_{2(|l|-m)-k_1}\left[\frac{\mathrm{i}B\omega(z)}{2}(p_{1x}-p_{2x})\right]\times$$
$$\mathrm{H}_{2(|l|-m)-e}\left[\frac{\mathrm{i}B\omega(z)}{2}(p_{1y}-p_{2y})\right]\sum_{f=0}^{k_1/2}(-1)^f\frac{k_1!}{f!(k_1-2f)!}\left[\mathrm{i}(A-B)\omega(z)\right]^{k_1-2f}\times$$
$$\exp\left\{\frac{\left[\frac{B}{2}(p_{1x}+p_{2x})-C(p_{1x}-p_{2x})+D(p_{1x}-p_{2x})\right]^2}{4E}\right\}\times$$
$$\mathrm{H}_{2m+|l|-s+k_1-2f}\left\{\mathrm{i}\left[\frac{\frac{B}{2}(p_{1x}+p_{2x})-C(p_{1x}-p_{2x})+D(p_{1x}-p_{2x})}{2\sqrt{E}}\right]\right\}\times\sum_{g=0}^{e/2}(-1)^g\frac{e!}{g!(e-2g)!}\left[\mathrm{i}(A-B)\omega(z)\right]^{e-2g}\times$$
$$\exp\left\{\frac{\left[\frac{B}{2}(p_{1y}+p_{2y})-C(p_{1y}-p_{2y})+D(p_{1y}-p_{2y})\right]^2}{4E}\right\}\times\mathrm{H}_{2m+s+e-2g}\left\{\mathrm{i}\left[\frac{\frac{B}{2}(p_{1y}+p_{2y})-C(p_{1y}-p_{2y})+D(p_{1y}-p_{2y})}{2\sqrt{E}}\right]\right\},\tag{17}$$

式中：k_1、e、f、g 为大于等于 0 的整数；$A=\frac{-\mathrm{i}kz}{z^2+z_{\mathrm{R}}^2}$，$B=\frac{\mathrm{i}k}{z}$，$C=\frac{1}{\rho_0^2}$，$D=\frac{(A-B)B\omega^2(z)}{4}$，$E=\frac{1}{2\omega^2(z)}+\frac{2}{\rho_0^2}-\frac{1}{\rho_{\mathrm{h}}^2}-\frac{(A-B)^2\omega^2(z)}{8}$。

令 $\boldsymbol{p}=\boldsymbol{p}_1=\boldsymbol{p}_2$，则接收端 C 任一点的平均光强表达式为

$$\left\langle I(\boldsymbol{p},z)\right\rangle=\Gamma(\boldsymbol{p},\boldsymbol{p},z)=\left[\frac{k^3\sigma_{\mathrm{h}}}{\pi\sqrt{\pi}\,z^2(|l|)!}\right]\frac{2^{-4|l|}}{\omega^{2|l|+2}(z)}\cdot\frac{\mathrm{i}^{-3|l|}}{\left(\sqrt{E}\right)^{|l|+2}}\times$$
$$\sum_{m=0}^{|l|}\sum_{s=0}^{|l|}\sum_{k_1=0}^{2(|l|-m)}\sum_{e=0}^{2(|l|-m)}\begin{bmatrix}|l|\\m\end{bmatrix}\begin{bmatrix}|l|\\s\end{bmatrix}\begin{bmatrix}2(|l|-m)\\k_1\end{bmatrix}\begin{bmatrix}2(|l|-m)\\e\end{bmatrix}\times$$
$$\frac{2^{-2m}}{\left(\sqrt{E}\right)^{4m}}\cdot\frac{\left[-\mathrm{i}\mathrm{sgn}(l)\right]^{(s)}}{\left[\sqrt{\frac{2}{\omega^2(z)}}\right]^{2(|l|-m)+1}}\cdot\frac{(2\mathrm{i})^{-k_1+2f-e+2g}}{\left(\sqrt{E}\right)^{k_1-2f+e-2g}}\mathrm{H}_{2(|l|-m)-k_1}(0)\mathrm{H}_{2(|l|-m)-e}(0)\times$$
$$\sum_{f=0}^{k_1/2}(-1)^f\frac{k_1!}{f!(k_1-2f)!}\left[\mathrm{i}(A-B)\omega(z)\right]^{k_1-2f}\exp\left[\frac{(Bp_x)^2}{4E}\right]\times\mathrm{H}_{2m+|l|-s+k_1-2f}\left[\mathrm{i}\left(\frac{Bp_x}{2\sqrt{E}}\right)\right]\times$$
$$\sum_{g=0}^{e/2}(-1)^g\frac{e!}{g!(e-2g)!}\left[\mathrm{i}(A-B)\omega(z)\right]^{e-2g}\exp\left[\frac{(Bp_y)^2}{4E}\right]\times\mathrm{H}_{2m+s+e-2g}\left[\mathrm{i}\left(\frac{Bp_y}{2\sqrt{E}}\right)\right],\tag{18}$$

式中：$\boldsymbol{p}=(p_x,p_y)$ 为接收端光场的二维坐标点。

2.2　接收端散斑光场复相干度

空间相干特性是回波特性的一个重要组成部分，可以反映回波光场在空间两点的相干性强弱，一般用光束空间复相干度（DOC）表示。海洋湍流中 LG 光束经高斯随机粗糙面散射后回波光场的复相干度[36] γ 为

$$\gamma(\Delta\boldsymbol{p})=\frac{\left\langle U_{\mathrm{C}}(\boldsymbol{p}_1)U_{\mathrm{C}}^*(\boldsymbol{p}_2)\right\rangle}{\sqrt{\left\langle I(\boldsymbol{p}_1)\right\rangle\left\langle I(\boldsymbol{p}_2)\right\rangle}},\tag{19}$$

式中：$\Delta\boldsymbol{p}=\boldsymbol{p}_1-\boldsymbol{p}_2$。

3　仿真结果与分析

根据第 2 节的理论推导，对海洋湍流中 LG 光束经高斯随机粗糙面的回波散射光场的复相干度进行数值仿真。由于蓝绿激光在水中的衰减小、传输远，可以抑制湍流效应，而粗糙面对蓝绿波段的 LG 光束有散射效果，并考虑到海洋湍流太强会严重破坏 LG 光束的光斑和光场相干性，为了更加直观地观察复相干度受粗糙面散射的影响，因此采用弱海洋湍流，选取的仿真参数如表 1 所示。为方便起见，无特殊说明时仿真参数如表 1 所示。

表 1　数值仿真参数

Table 1　Numerical simulation parameters

Parameter	Value	Parameter	Value
λ	532 nm	ρ_{h}	20 mm
ω_0	10 mm	C_n^2	10^{-16}
z	50 m	χ_{T}	10^{-9} K^2•s^{-1}
ρ_0	0.02 m	ε	10^{-3} m^2•s^{-3}
σ_{h}	0.5λ	ω	−4

3.1　光源参数对回波光场复相干度的影响

图 4 所示为回波光场复相干度随 LG 光束拓扑荷数的变化曲线，x 方向的相关间隔为 $\Delta p_x=p_{1x}-p_{2x}$。从图 4 可以看出，拓扑荷数 l 越大，复相干度 γ 越小。这是因为随着拓扑荷数的增加，LG 光束的光斑面积变大，相位涡旋也逐渐变多，在传输过程中相位受粗糙面和海洋湍流的扰动就越大。这一结论与大气湍流中光束的拓扑荷数对复相干度的影响规律一致[24]。

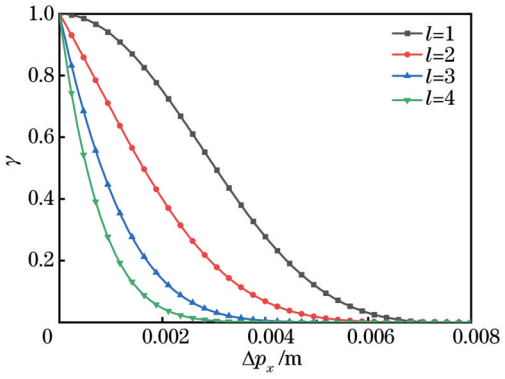

图 4　复相干度随拓扑荷数的变化曲线

Fig. 4　DOC of the echo field at different topological charges

图 5 所示为当拓扑荷数为 2 时，回波光场复相干度随 LG 光束束腰半径的变化曲线。从图 5 可以看出，当束腰半径 $\omega_0=1$ mm 时，复相干度 γ 曲线的宽度最大，

随着束腰半径的增加，复相干度曲线的下降趋势愈来愈明显。这是因为照射在粗糙面上的光斑面积会随着束腰半径的增大而增大，且中心暗核区域的面积也随之增大，散射效果越来越强，对LG光束的相干性破坏越大。这个结果可以应用在海洋目标探测和识别领域中，通过改变拓扑荷数和束腰半径来降低海洋湍流对光束传输的影响。

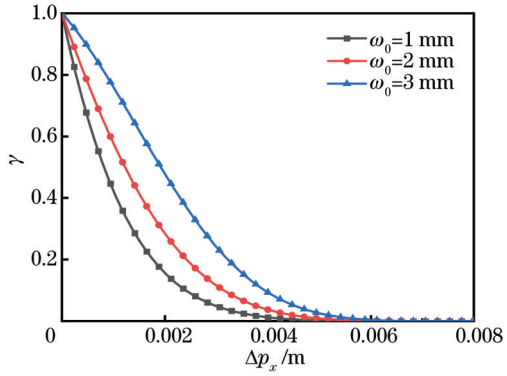

图5　复相干度随束腰半径的变化曲线

Fig. 5　DOC of the echo field at different waist radii

图6所示为当拓扑荷数为2时，回波光场复相干度随LG光束波长的变化曲线。从图6可以看出，复相干度随着LG光束波长的增加逐渐减小。这是因为回波光场的复相干度受粗糙面和海洋湍流的共同作用，波长较长的光束受海洋湍流和粗糙面的影响大于波长较短的光束。

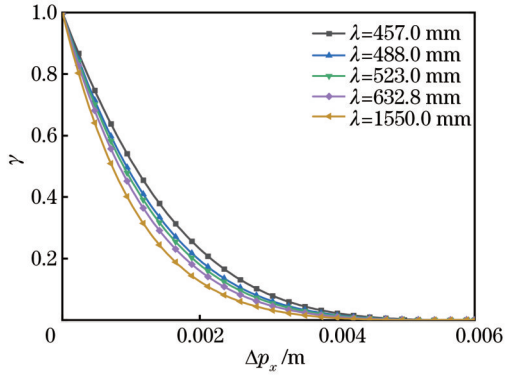

图6　复相干度随波长的变化曲线

Fig. 6　DOC of the echo field at different wavelengths

图7所示为当拓扑荷数为2时，不同传输距离对回波光场复相干度的影响。随着传输距离z的增大，复相干度逐渐减小。这是因为传输距离z越长，海洋湍流对LG光束的相位扰动越强，导致复相干度逐渐降低。

3.2　海洋湍流对回波光场复相干度的影响

进一步对不同海洋湍流强度下的回波光场复相干度γ进行仿真。从图8可以看出，随着温度方差耗散率χ_T的增大，湍流增强，复相干度γ逐渐减小。从图9可以发现，动能耗散率ε越小，湍流越强，复相干度γ越小，表明LG光束经高斯随机粗糙面散射过程中，海洋湍流作为传输介质，会影响LG光束的相干性，且湍流越强，对LG光束相干性的破坏越大。

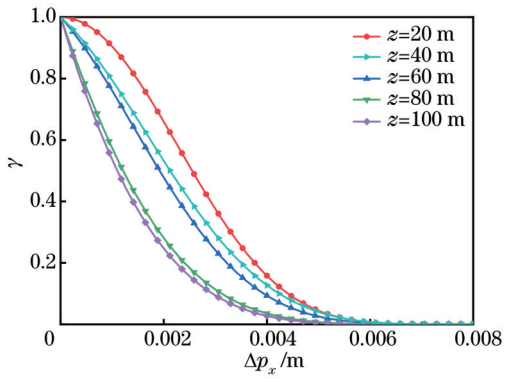

图7　复相干度随传输距离的变化曲线

Fig. 7　DOC of the echo field at different transmission distances

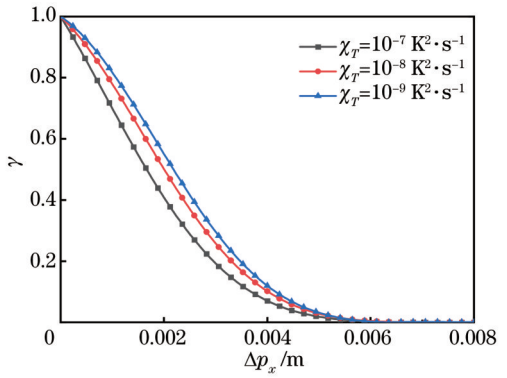

图8　复相干度随温度方差耗散率的变化曲线

Fig. 8　DOC of the echo field at different dissipation rates of mean-squared temperature

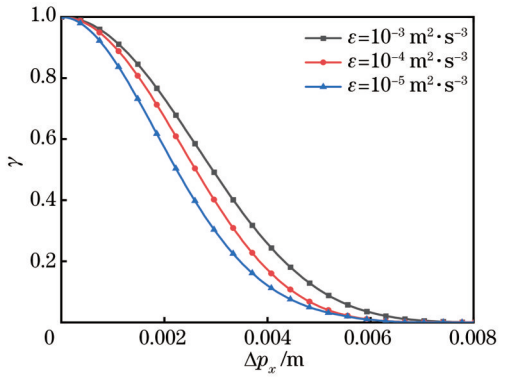

图9　复相干度随湍流动能耗散率的变化曲线

Fig. 9　DOC of the echo field at different turbulent kinetic energy dissipation rates

3.3　高斯随机粗糙面对回波光场复相干度的影响

图10所示为粗糙面相干长度对接收端光场复相干度的影响，仿真参数如表1所示。从图10可以看出，回波光场的复相干度γ随x轴相关间隔Δp_x的增大逐

渐下降，并且随着粗糙面相干长度ρ_h的增大逐渐增大。这是因为当其他因素不变时，ρ_h越大，粗糙面越平缓，对光束相位扰动越小，则复相干度γ越大。当粗糙面的ρ_h大于光束在湍流中传输的相干长度ρ_0时，回波光场的复相干度γ没有明显变化，这是因为当$\rho_h \geqslant \rho_0$时，相比海洋湍流，粗糙面对接收端光场复相干度γ的影响较小，此时γ主要受海洋湍流的影响；当$\rho_h < \rho_0$时，γ受海洋湍流和高斯随机粗糙面共同影响。

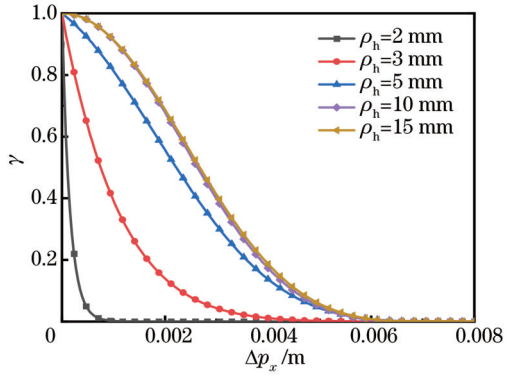

图 10 不同粗糙面相干长度下接收端的复相干度（ρ_0=0.01 m）

Fig. 10 DOC of the echo field at different coherence lengths of rough surface (ρ_0=0.01 m)

4 结 论

采用广义 Huygens-Fresnel 衍射原理，利用涡旋光束特殊的螺旋相位特性在抑制湍流效应方面的相对优势，推导出海洋湍流中 LG 光束经粗糙面的回波散射光强解析表达式，进一步得到接收端回波散射光场复相干度的理论表达式，并探讨了复相干度和光源参数、海洋湍流强度以及粗糙面参数的关系。仿真结果表明：回波光场复相干度随着 LG 光束拓扑荷数的增大、束腰半径的增大、波长的增大以及传输距离的增大而逐渐减小，随海洋湍流的增强逐渐减小；粗糙面的相干长度越大，粗糙面越光滑，复相干度随着粗糙面相干长度的增大而减小。当粗糙面的相干长度大于或等于光束在海洋湍流中传输的相干长度时，粗糙面对光场复相干度的影响相比海洋湍流的影响可以忽略；当粗糙面的相干长度小于光束在海洋湍流中传输的相干长度时，复相干度受海洋湍流和粗糙面共同影响。粗糙面的均方根粗糙度对复相干度无影响。考虑到涡旋光场相对于高斯光场的复杂性和双向传播路径的复杂性，对传播路径使用 Rytov 近似，这大大简化了回波散射光强封闭表达式的计算过程，对海洋湍流中涡旋光束回波特性的研究将考虑传播路径和回波路径上的实时干扰。所推导的海洋湍流中 LG 光束经粗糙面的回波散射光场解析表达式和回波光场的复相干度，可为水下目标探测等提供参考。

参 考 文 献

[1] 韦育，于永河，黑小兵，等. 涡旋光束和光子计数在水下光通信中的应用[J]. 激光与光电子学进展，2022，59(13)：1301001.
Wei Y，Yu Y H，Hei X B，et al. Application of vortex beam and photon counting in underwater optical communication[J]. Laser & Optoelectronics Progress，2022，59(13)：1301001.

[2] 唐军武，朱培志，刘秉义，等. 海洋剖面激光雷达探测中颗粒物偏振散射问题[J]. 光学学报，2022，42(12)：1200001.
Tang J W，Zhu P Z，Liu B Y，et al. Polarized light scattering of particulate matter in detection of oceanographic profiling LiDAR [J]. Acta Optica Sinica，2022，42(12)：1200001.

[3] 王明军，张佳琳，王主玉，等. 水下悬浮球形藻类粒子群对拉盖尔-高斯涡旋光束的散射[J]. 光学学报，2022，42(18)：1829001.
Wang M J，Zhang J L，Wang Z Y，et al. Scattering of Laguerre-Gaussian vortex beams by underwater suspended spherical algal particle swarms[J]. Acta Optica Sinica，2022，42(18)：1829001.

[4] Liu D J，Wang G Q，Yin H，et al. Propagation properties of a partially coherent anomalous hollow vortex beam in underwater oceanic turbulence[J]. Optics Communications，2019，437：346-354.

[5] Liu X Y，Zhou G Q，Shen Y T. Effect of oceanic turbulence with anisotropy on the propagation of multi-sinc Schell-model beams[J]. Results in Physics，2022，36：105447.

[6] Ata Y，Baykal Y. Scintillations of optical plane and spherical waves in underwater turbulence[J]. Journal of the Optical Society of America A，2014，31(7)：1552-1556.

[7] Wang Z Q，Zhang P F，Qiao C H，et al. Scintillation index of Gaussian waves in weak turbulent ocean[J]. Optics Communications，2016，380：79-86.

[8] Farwell N，Korotkova O. Intensity and coherence properties of light in oceanic turbulence[J]. Optics Communications，2012，285(6)：872-875.

[9] Zhang J L，Kou L L，Yang Y，et al. Monte-Carlo-based optical wireless underwater channel modeling with oceanic turbulence [J]. Optics Communications，2020，475：126214.

[10] 刘娜，柯杰耀，杨苏辉，等. 载波调制高斯脉冲激光水下传输特性的仿真分析[J]. 光学学报，2018，38(4)：0401003.
Liu N，Ke J Y，Yang S H，et al. Simulation and analysis on underwater transmission characteristics of Gaussian pulse lasers with carrier modulation[J]. Acta Optica Sinica，2018，38(4)：0401003.

[11] 李坤，杨苏辉，廖英琦，等. 强度调制 532 nm 激光水下测距[J]. 物理学报，2021，70(8)：084203.
Li K，Yang S H，Liao Y Q，et al. Underwater ranging with intensity modulated 532 nm laser source[J]. Acta Physica Sinica，2021，70(8)：084203.

[12] Coullet P，Gil L，Rocca F. Optical vortices[J]. Optics Communications，1989，73(5)：403-408.

[13] 马志远，陈康，张明明，等. 拉盖尔-高斯幂指数相位涡旋光束传输特性[J]. 光学学报，2022，42(5)：0526001.
Ma Z Y，Chen K，Zhang M M，et al. Propagation characteristics of Laguerre-Gaussian power-exponent-phase-vortex beams[J]. Acta Optica Sinica，2022，42(5)：0526001.

[14] Wang L Y，Ma J T，Xiao M，et al. Application of optical orbital angular momentum to rotation measurements[J]. Results in Optics，2021，5：100158.

[15] Jiang Y X，Li Z H. Monte Carlo simulation of Mueller matrix of randomly rough surfaces[J]. Optics Communications，2020，474：126113.

[16] Freund I. Joseph W. Goodman：speckle phenomena in optics：theory and applications[J]. Journal of Statistical Physics，2008，130(2)：413-414.

[17] Ogilvy J A，Merklinger H M. Theory of wave scattering from random rough surfaces[J]. The Journal of the Acoustical Society

of America, 1991, 90(6): 3382.
[18] 刘曼. 涡旋光束形成的散斑场光强和相位的分布特性[J]. 光学学报, 2014, 34(11): 1126001.
Liu M. Distribution properties of intensity and phase of speckle fields produced by vortex beam[J]. Acta Optica Sinica, 2014, 34(11): 1126001.
[19] Liu M, Song H S, Chen X Y, et al. Intensity distribution and phase vortices of speckle fields generated by multi-aperture random scattering screens[J]. Chinese Physics Letters, 2010, 27(3): 034202.
[20] Holmes J F, Lee M H, Kerr J R. Effect of the log-amplitude covariance function on the statistics of speckle propagation through the turbulent atmosphere[J]. Journal of the Optical Society of America A, 1980, 70(4): 355-360.
[21] Cui C, Wang Z, Zhan X K, et al. Measurement of the adjustable slight roughness emulated by a spatial light modulator employing the vortex beam speckle pattern[J]. Applied Optics, 2020, 59(12): 3630-3635.
[22] Li Y Q, Wu Z S. Statistical characteristics of a Gaussian beam reflected by a retro-reflector in atmospheric turbulence[J]. Optik, 2018, 158: 1361-1369.
[23] Li Y Q, Wang L G, Wu Z S. Numerical simulation for echo characteristics of laser beams reflected by retro-reflectors in atmospheric turbulence[J]. Optik, 2019, 179: 244-251.
[24] Li Y Q, Wang L G, Gong L, et al. Speckle characteristics of vortex beams scattered from rough targets in turbulent atmosphere[J]. Journal of Quantitative Spectroscopy and Radiative Transfer, 2020, 257: 107342.
[25] 李艳玲, 梅海平, 任益充, 等. 湍流大气中随机粗糙表面激光回波空间相干性仿真[J]. 物理学报, 2022, 71(14): 140201.
Li Y L, Mei H P, Ren Y C, et al. Simulation of spatial coherence of laser echo light field from random rough surface in turbulent atmosphere[J]. Acta Physica Sinica, 2022, 71(14): 140201.
[26] 张凯宁, 刘永欣, 蒲继雄. 涡旋光束在海洋湍流中传输的闪烁因子[J]. 中国激光, 2019, 46(7): 0705001.
Zhang K N, Liu Y X, Pu J X. Scintillation index of vortex beams propagating in oceanic turbulence[J]. Chinese Journal of Lasers, 2019, 46(7): 0705001.
[27] 卢腾飞, 刘永欣, 蒲继雄. 涡旋光束在水下湍流中传输的闪烁因子的实验研究[J]. 光子学报, 2019, 48(12): 1214004.
Lu T F, Liu Y X, Pu J X. Experimental study on scintillation index of vortex beam propagation in underwater turbulence[J]. Acta Photonica Sinica, 2019, 48(12): 1214004.
[28] 潘孙翔, 赵生妹, 王乐, 等. 水下轨道角动量态传输特性的实验研究[J]. 光学学报, 2018, 38(6): 0606004.
Pan S X, Zhao S M, Wang L, et al. Experimental investigation of underwater propagation characteristics of orbital angular momentum[J]. Acta Optica Sinica, 2018, 38(6): 0606004.
[29] Allen L, Beijersbergen M W, Spreeuw R J, et al. Orbital angular momentum of light and the transformation of Laguerre-Gaussian laser modes[J]. Physical Review A, 1992, 45(11): 8185-8189.
[30] 李晓庆, 赵琦, 季小玲. Rytov 相位结构函数二次近似和硬边光阑复高斯函数展开近似的验证[J]. 光学学报, 2011, 31(12): 1201002.
Li X Q, Zhao Q, Ji X L. Confirmation of the quadratic approximation of Rytov phase structure function and the approximation of complex Gaussian-function expansion of hard-edge apertures[J]. Acta Optica Sinica, 2011, 31(12): 1201002.
[31] Pan Y Q, Zhao M L, Zhang M M, et al. Propagation properties of rotationally-symmetric power-exponent-phase vortex beam through oceanic turbulence[J]. Optics & Laser Technology, 2023, 159: 109024.
[32] Wang L G, Gao M, Li Y Q, et al. Intensity fluctuations of reflected wave from a diffuse target with a hard edge in atmospheric turbulence[J]. Journal of Quantitative Spectroscopy and Radiative Transfer, 2017, 195: 141-146.
[33] Xiang N J, Wu Z S, Guo Q F, et al. Backscatter amplification effect for a reflected partially coherent Gaussian beam in turbulent medium[J]. Journal of Quantitative Spectroscopy and Radiative Transfer, 2015, 163: 1-6.
[34] Cheng M J, Guo L X, Li J T, et al. Propagation of an optical vortex carried by a partially coherent Laguerre-Gaussian beam in turbulent ocean[J]. Applied Optics, 2016, 55(17): 4642-4648.
[35] Gradshteyn I S, Ryzhik I M. Table of integrals, series, and products [M]. 7th ed. Amsterdam: Academic Press, 2007.
[36] 王利国, 吴振森, 王明军. 湍流大气中的有限孔径平面镜反射波的二阶统计特性[J]. 光学学报, 2013, 33(11): 1101002.
Wang L G, Wu Z S, Wang M J. Second-order statistics for wave reflected by a plane mirror with a finite aperture[J]. Acta Optica Sinica, 2013, 33(11): 1101001.

Echo Characteristics of Vortex Beam Passing Through Rough Surface Under Oceanic Turbulence

Wu PengFei[1*], Zhang Mi[1], Wang Jiao[2], Tan ZhenKun[3]

[1]*School of Automation and Information Engineering, Xi'an University of Technology, Xi'an* 710048, *Shaanxi, China*;

[2]*School of Electronic Information and Artificial Intelligence, Shaanxi University of Science and Technology, Xi'an* 710021, *Shaanxi, China*;

[3]*School of Opto-Electronical Engineering, Xi'an Technological University, Xi'an* 710021, *Shaanxi, China*

Abstract

Objective The surface of the object which in nature is rough relative to the wavelength of light beams is a rough target. When the light is incident on the rough target, the beam will be scattered, and the receiving end will receive the light intensity pattern of alternating light and dark waves, which is called speckle pattern. The echo scattering characteristic of the light field is one of the key technologies for the integration of underwater laser communication and detection in the

future. In ocean detection technology, underwater scattering technology, and underwater wireless optical communication technology, the transmission characteristics of beams through oceanic turbulence and echo characteristics of beams through the rough surface play a crucial role in turbulent conditions. The physical characteristics of the rough target surface (surface roughness, coherence length, deformation degree, motion velocity, and rotation velocity) play an important role in influencing echo characteristics. The current studies mainly adopt the fractal method, wavelet transform, deep learning, and other methods to process the laser speckle pattern collected at the receiving end. The surface roughness, deformation degree, translation velocity, and rotation velocity of the rough target can be identified. The current underwater detection technology is mainly laser, but the laser loss during detection is serious, thus resulting in limited rough target information reflected by the received speckle. Since the vortex beam features hollow intensity distribution, phase helix, and orthogonality of orbital angular momentum (OAM), it can carry more information than the Gaussian beam. Laguerre-Gaussian (LG) beams are typical vortex beams with significant advantages in light scattering and target recognition. At present, there are two aspects to study the scattering characteristics of light beams through rough targets. The first is the speckle characteristics of light beams through the rough surface in free space, and the second is the speckle characteristics of light beams through the rough surface in atmospheric turbulence. The propagation theory of vortex beams through oceanic turbulence is very mature, but the scattering characteristics of vortex beams through Gaussian random rough surface in weak oceanic turbulence are rarely studied.

Methods Spatial coherence property is a part of the echo scattering property, which can reflect the coherence of the echo field between two points in space. The spatial complex coherence degree of the beam is utilized to represent the spatial coherence property of the echo field. The spatial distribution of the speckle is related to the surface coherence length of the rough target. We build a double-path transmission model of LG beam through Gaussian random rough surface in weak oceanic turbulence by referring to the scattering characteristics of vortex beams through the rough surface in atmospheric turbulence. Based on the generalized Huygens-Fresnel diffraction principle, the intensity of the echo speckle field of LG beams reflected by a rough surface with Gaussian distribution in oceanic turbulence is derived. The influences of the LG beam′s light source parameters, oceanic turbulence intensity, and rough surface roughness on speckle field complex coherence degree are investigated.

Results and Discussions The effects of light source parameters, oceanic turbulence, and rough target surface parameters on the complex coherence of the echo speckle field are analyzed numerically. Figs. 4-10 show that complex coherence decreases with the increasing topological charge, waist radius, and wavelength of LG beams, decreases with the increase in oceanic turbulence intensity, and rises with the increasing coherence length of the rough surface. Additionally, when the coherent length of the rough surface is larger than that of spherical wave propagating in oceanic turbulence, the complex coherence degree does not change significantly. This shows that the influence of rough surfaces on complex coherence is much less than that of oceanic turbulence.

Conclusions This study is based on the generalized Huygens-Fresnel diffraction principle and the relative advantages of vortex beams in suppressing turbulence effect due to the special helical phase characteristics of the beams. Then the analytical expression of the scattering intensity of LG beams through the rough surface in oceanic turbulence is innovated, and the theoretical expression of the complex coherence of the scattering field at the receiving end is obtained. The results indicate that the complex coherence decreases with the increasing topology charge, waist radius, and wavelength of the LG beam, decreases with the rising oceanic turbulence intensity, and rises with the increasing dry length of the rough surface. However, when the coherent length of the rough surface is larger than that of the spherical wave propagating in oceanic turbulence, the complex coherence degree does not change significantly. This shows that the influence of rough surfaces on complex coherence is much less than that of oceanic turbulence. The analytical expression of the light field scattered by LG beams through the rough surface and the complex coherence of the light field of the back wave derived in this paper provides a theoretical basis for underwater target detection.

Key words oceanic optics; oceanic turbulence; Laguerre-Gaussian beam; speckle; echo characteristics; complex coherence degree